ARTHRITIS & RHEUMATOLOGY
Vol. 66, No. 8, August 2014, pp 2270–2280
DOI 10.1002/art.38646

Deletion of the Antiphospholipid Syndrome Autoantigen β_2-Glycoprotein I Potentiates the Lupus Autoimmune Phenotype in a Toll-like Receptor 7–Mediated Murine Model

Bill Giannakopoulos,[1] Peyman Mirarabshahi,[1] Miao Qi,[1] Chris Weatherall,[1] Jian Cheng Qi,[1] Kumiko Tanaka,[1] Ewan Millar,[2] Leon Vonthethoff,[1] Dominique Gatto,[3] Derek Spielman,[4] and Steven A. Krilis[1]

Objective. **The BXSB.*Yaa* mouse strain is a model of systemic lupus erythematosus that is dependent on duplication of the Toll-like receptor 7 gene. The objective of this study was to systematically describe the amplified autoimmune phenotype observed when the soluble plasma protein β_2-glycoprotein I (β_2GPI) gene was deleted in male BXSB.*Yaa* mice.**

Methods. **We generated BXSB.*Yaa* and NZW mouse strains in which the β_2GPI gene had been knocked out by backcrossing the wild-type strains with C57BL/6 β_2GPI$^{-/-}$ mice for 10 generations. Sex- and age-matched mice of the various strains were housed under identical conditions and were killed at fixed time intervals. Serum and tissue specimens were collected at various time points. Lupus-associated autoantibodies, inflammatory cytokines, and the type I interferon (IFN) gene signature were measured. Flow cytometric analyses of lymphocyte populations were performed. The severity of glomerulonephritis was graded by 2 independent renal histopathologists.**

Results. **Male BXSB.*Yaa* β_2GPI$^{-/-}$ mice developed significant lymphadenopathy and splenomegaly compared with age-matched controls. Male BXSB.*Yaa* β_2GPI$^{-/-}$ mice also had significantly higher levels of autoantibodies, increased levels of inflammatory cytokines including tumor necrosis factor α, interleukin-6, and BAFF, and more severe glomerulonephritis. The type I IFN gene signature in male BXSB.*Yaa* β_2GPI$^{-/-}$ mice was significantly higher than that in control mice. Male BXSB.*Yaa* β_2GPI$^{-/-}$ mice also had marked dysregulation of various B cell and T cell populations in the spleens and lymph nodes and a disturbance in apoptotic cell clearance.**

Conclusion. **Deletion of β_2GPI accelerates and potentiates the autoimmune phenotype in male BXSB.*Yaa* mice.**

The antiphospholipid syndrome (APS) is an autoantibody-mediated disorder characterized by thrombosis and obstetric complications (1,2). The main antigen in APS is β_2-glycoprotein I (β_2GPI), an abundant soluble plasma protein produced by the liver that can bind to anionic phospholipids (3). Anti-β_2GPI autoantibodies are commonly referred to as antiphospholipid antibodies. β_2GPI is composed of 5 domains (4).

Supported by a project grant from the National Health and Medical Research Council of Australia to Drs. Giannakopoulos and Krilis and an establishment grant by The St. George and Sutherland Medical Research Foundation to Dr. Giannakopoulos. Dr. Mirarabshahi is recipient of an Australian Postgraduate Award.

[1]Bill Giannakopoulos, MB BS, PhD, FRACP, Peyman Mirarabshahi, MD, PhD, Miao Qi, MSc, Chris Weatherall, MB BS, PhD, FRACP, Jian Cheng Qi, MD, PhD, Kumiko Tanaka, PhD, Leon Vonthethoff, MB BS, Steven A. Krilis, MB BS, PhD, FRACP: St. George Hospital and University of New South Wales, Kogarah, New South Wales, Australia; [2]Ewan Millar, MB BS: St. George Hospital, Kogarah, New South Wales, Australia, Kinghorn Cancer Centre and Garvan Institute of Medical Research, Darlinghurst, New South Wales, Australia, University of Western Sydney, Campbelltown Campus, Campbelltown, New South Wales, Australia, and University of New South Wales, Kensington, New South Wales, Australia; [3]Dominique Gatto, PhD: Garvan Institute of Medical Research and St. Vincent's Clinical School, University of New South Wales, Darlinghurst, New South Wales, Australia; [4]Derek Spielman, MVSc, PhD: University of Sydney, Camperdown Campus, Camperdown, New South Wales, Australia.

Drs. Giannakopoulos and Mirarabshahi contributed equally to this work.

Address correspondence to Steven A. Krilis, MB BS, PhD, Department of Infectious Diseases, Immunology and Sexual Health, St. George Hospital, University of New South Wales, 2 South Street, Kogarah, Sydney NSW 2217, Australia. E-mail: s.krilis@unsw.edu.au.

Submitted for publication November 13, 2013; accepted in revised form March 25, 2014.

The first 4 domains of β_2GPI are similar and contain 2 disulfide bridges each, whereas the fifth domain at the C-terminus is distinct, because it contains an extra disulfide bond (4). This extra disulfide bond participates in oxidoreductase reactions (5), and when it is in the free thiol form (the predominant form in healthy individuals) (6), it can protect endothelial cells against oxidative stress–induced apoptosis (7). β_2GPI can bind to apoptotic cells via the cell surface–expressed Ro 60 molecule (8) and may mediate a role in apoptotic cell clearance (9,10).

Forty percent of patients with APS also have systemic lupus erythematosus (SLE) (11), and autoantibodies to β_2GPI develop in 36% of patients with SLE (12), suggesting that there may be an overlap in the pathogenic pathways contributing to the development of anti-β_2GPI autoantibodies in APS and SLE. The possibility of an overlapping mechanism linking the pathogenesis of APS and that of SLE is further raised by observing the spontaneous development of autoantibodies against domain I of β_2GPI (identical to APS patient anti-β_2GPI autoantibody epitope specificity) and a syndrome analogous to human APS in male (NZW $\times$ BXSB)F1 mice, the only known murine model of spontaneous APS described to date (13–15). Neither NZW nor BXSB.*Yaa* mice develop anti-β_2GPI autoantibodies or an APS syndrome, although both strains of mice develop the lupus phenotype via distinct genetic abnormalities (16).

Male BXSB mice develop a lupus phenotype due to translocation of the Y-linked autoimmune accelerator (YAA) from the X chromosome to the Y chromosome. There are multiple genes on the YAA translocation, although the strongest evidence has implicated duplication of the Toll-like receptor 7 (TLR-7) gene as being mostly responsible for the lupus phenotype in this strain of mice (17,18).

In studies delineating the pathogenesis of SLE, dysregulated activation of TLR-7 within B lymphocytes and plasmacytoid dendritic cells (DCs) by small nuclear RNPs contained within autoantibody immune complexes (e.g., Sm and Ro/SSA) and the subsequent production of type I interferon (IFN) have been implicated as an important pathway contributing to the development of disease, sustaining the generation of more autoantibodies (19,20). We generated β_2GPI-knockout mice in the lupus autoimmune strains NZW and BXSB.*Yaa* as part of a larger project to delineate the influence of the β_2GPI autoantigen on the (NZW $\times$ BXSB.*Yaa*)F1 phenotype. In this study, we systematically describe an accelerated lupus phenotype that emerged when the β_2GPI gene was deleted in male BXSB.*Yaa* mice.

MATERIALS AND METHODS

BXSB.*Yaa*, NZW, and C57BL/6 mice were obtained from The Jackson Laboratory. BXSB.*Yaa* β_2GPI$^{-/-}$ and NZW β_2GPI$^{-/-}$ mice were derived by backcrossing C57BL/6 β_2GPI$^{-/-}$ mice for 10 generations with BXSB.*Yaa* and NZW wild-type (WT) mice, respectively; genotyping was performed using polymerase chain reaction (PCR) (21). Quantitation of the TLR-7 gene was performed by quantitative PCR, using genomic DNA, with results expressed relative to the C57BL/6 TLR-7 gene copy number. Ribosomal protein S13 (Qiagen) was used as the housekeeping gene. The *Tlr7* primer sequence used was as follows: forward GTACCAAGAGGCTGCAGATTAGAC and reverse TAGCCTCAAGGCTCAGAAGATG.

Animal studies were approved by the University of South Wales Animal Care and Ethics Committee. Sera from all mice were stored at −80°C until used. The kidneys, spleen, and lymph nodes were individually removed and stored either in 10% neutral buffered formalin for 1–2 weeks until paraffin embedding or were weighed, photographed, and measured, and some of the tissue specimens were snap-frozen in freezing medium by immersion in liquid nitrogen. For RNA extraction, small sections of spleen were incubated in RNAlater (Qiagen) for 24 hours at 4°C, and then stored at −80°C until used.

Autoantibody measurement. Assays from Alpha Diagnostic were performed to quantify antinuclear antibodies (ANAs) and semiquantitatively determine anti–double-stranded DNA (anti-dsDNA), anti-Ro/SSA, and anti-β_2GPI autoantibodies in murine serum samples, according to the manufacturer's instructions. Anticardiolipin (aCL) autoantibodies were quantitated using kits purchased from Vital Diagnostics, according to the manufacturer's instructions. Antioxidized RNA antibodies were measured with a specific enzyme-linked immunosorbent assay kit using 8-hydroxyguanosine conjugate (Cell Biolabs) according to the manufacturer's instructions.

Renal histology. Five-micrometer–thick frozen sections were cut from whole kidneys. Fluorescein isothiocyanate (FITC)–conjugated goat anti-mouse C3 (Immunology Consultants Laboratory) or rabbit anti-mouse IgG (Beckman Coulter) was added at 1:20 dilution in phosphate buffered saline (PBS) for 30 minutes at room temperature. The sections were washed in PBS for 5 minutes at room temperature and then coverslipped with fluorescent mounting medium (Dako). In the negative control, the primary antibody was omitted. For scoring, stained sections were viewed using a specialized fluorescence microscope, independently by 2 expert renal pathologists who were blinded to all details of the experiments. The intensity of staining was graded semiquantitatively from 0 to 3+ (indicating increasing severity) by assessing >100 glomeruli present in whole kidney sections.

Spleen immunofluorescence. Spleen sections (5–7 μm thick) were fixed with acetone and blocked with 30% horse serum. Sections were incubated with biotinylated anti-CD3 (eBioscience) followed by Alexa Fluor 555–conjugated streptavidin (Invitrogen), Alexa Fluor 647–conjugated anti-IgD (BioLegend), and FITC-conjugated anti-IgM (BD Biosciences).

Images were captured on a Zeiss Axio Vert 200M microscope at 10× magnification.

Cytokines. The levels of the cytokines interleukin-6 (IL-6), IL-10, monocyte chemotactic protein 1 (MCP-1), interferon-γ (IFNγ), tumor necrosis factor α (TNFα), and IL-12p70 in sera were measured with a Cytometric Bead Array (CBA) Mouse Inflammation Kit (BD Biosciences) according to the manufacturer's instructions. BAFF levels were measured using a Quantikine Mouse BAFF/BLyS/TNFSF13B Immunoassay (R&D Systems) according to the manufacturer's instructions.

Splenocytes (4×10^6/ml) from BXSB.*Yaa* β_2GPI$^{-/-}$ and age-matched control mice were prepared in RPMI 1640 culture medium (Invitrogen) and stimulated with the TLR-7 agonist R848 (1 μg/ml) and then incubated for 24 hours at 37°C. The level of MCP-1 secreted into the supernatant was measured using a CBA Mouse Inflammation Kit (BD Biosciences) according to the manufacturer's instructions.

Type I IFN gene signature. To measure type I IFN–related activity, we quantified the expression of interferon regulatory factor 4 (IRF-4), IRF-5, suppressor of cytokine signaling 1 (SOCS-1), and immunoresponsive gene 1 (IRG-1) (22). RNA was extracted from age-matched BXSB.*Yaa* β_2GPI$^{-/-}$ and BXSB.*Yaa* WT mouse spleen samples using an RNeasy Plus Mini Kit (Qiagen). Complementary DNA from RNA was generated using a QuantiTect Reverse Transcription Kit (Qiagen). Using real-time quantitative PCR, relative concentrations of the 4 different type I IFN signature genes were assessed. Ribosomal protein S13 (Qiagen) served as the housekeeping gene. Results are shown as the relative messenger RNA (mRNA) level normalized to the mRNA level in BXSB.*Yaa* β_2GPI$^{+/+}$ splenocytes.

The primer sequences used for the quantitative PCRs are as follows: for IRF-4, forward CTCTTCAAGGCTTGGGCATT and reverse TGCTCCTTTTTTGGCTCCCT; for IRG-1, forward CACTGGGTGGCAGATGCAG and reverse CTTCATGCTCTGAGTCCGGG. The primer sequences for IRF-5 and SOCS-1 are held in confidence by the manufacturer (Qiagen).

Flow cytometric analysis. The mice were weighed, killed by CO_2 inhalation, and bled out by cardiac puncture. Spleens and cervical and inguinal lymph nodes were carefully removed, stripped of fat, and placed on tissue paper moistened with saline to avoid drying before being weighed and photographed using a Canon EOS 450D DSLR camera with a 50-mm F1.4 EX DG HSM lens; editing was performed using Photoshop CS4. The wet weights of organs were determined by using an ultrasensitive balance.

Preparation of single-cell suspensions. Single-cell suspensions from individual organs were prepared in PBS supplemented with 2% fetal calf serum (Invitrogen) and 0.05% sodium azide (PBS/bovine serum albumin [BSA]) (Sigma). Tissues were minced and teased through a 70-μm cell strainer (BD Biosciences). To remove contaminating erythrocytes, the cell suspensions were lysed by incubation in chilled 150 m*M* NH_4Cl, 10 m*M* $KHCO_3$ and 0.1 m*M* EDTA for 1 minute. The cells were then washed twice in PBS/BSA, and total cell numbers were determined using a Neubauer chamber. Viable cells were assessed by trypan blue exclusion.

Immunostaining and acquisition. Single-cell suspensions from lymph nodes and spleens were washed with PBS containing 0.5% BSA (Sigma) and 0.1% sodium azide (Sigma). Nonspecific binding was blocked using PBS/BSA containing rat anti-mouse CD16/CD32 monoclonal antibodies (Mouse BD Fc Block; BD Biosciences) and incubated for 20 minutes at room temperature. Cells (1×10^6) were suspended in 50 μl of PBS/BSA and incubated for 15 minutes at room temperature with the following antibodies: anti-CD23, anti-CD21/CD35, anti-CD11b, anti-CD11c, anti-CD45R (B220), anti-IgD, anti-IgM, anti-CD38, anti-CD44, anti-CD69, anti-CD62L, anti-CD4, anti-CD8, and anti-CD3. All antibodies were used at 0.5 μg per 10^6 cells. All of the antibodies were purchased from BD Biosciences, except anti-CD45R (B220) (Invitrogen) and anti-CD11c (Miltenyi Biotec).

The cells were washed with PBS/BSA and centrifuged at 240*g* for 3 minutes. The supernatant was discarded, the cells were resuspended in 0.5% paraformaldehyde fixative (Sigma), and the samples were stored at 4°C in the dark until analysis with a flow cytometer, which was performed within 3–4 hours of immunostaining. The cells were analyzed using a BD LSR II System (BD Biosciences) and FlowJo version 9.5 software (TreeStar). Forward light scatter and side light scatter panels were used for leukocyte gating. Selected populations were further analyzed based on the expression level of specific cell markers.

Apoptotic cell phagocytosis experiments. Thymocytes from 6–8-week-old BXSB.*Yaa* β_2GPI$^{-/-}$ mice were stained using a PKH26 Red Fluorescent Cell Linker Mini Kit (Sigma), which is a cell membrane–labeling kit. To induce apoptosis, stained cells were incubated for 3 hours in serum-free RPMI 1640 (Invitrogen) containing 1 μ*M* dexamethasone (Sigma). An Annexin V–FITC Apoptosis Detection Kit (BD Biosciences) was used to confirm and measure induction of apoptosis. After the stained cells were washed, a suspension of 5×10^6 cells/ml in 500 μl of PBS was injected intraperitoneally into 12–14-week-old male BXSB.*Yaa* β_2GPI$^{-/-}$ and BXSB.*Yaa* WT mice. After 1.5 hours, the mice were killed, and peritoneal cells were collected by injection of 5 ml of PBS into the peritoneal cavity and, after 5 minutes, aspirated. FITC-conjugated CD11b antibody (BD Biosciences) was used to stain monocyte/macrophages in the peritoneal cell suspension, and flow cytometric analysis of cells was carried out using a FACSCalibur system (BD Biosciences).

Statistical analysis. Data were analyzed using GraphPad Prism software. Data with a parametric distribution were analyzed using Student's *t*-test, data with a nonparametric distribution were analyzed using a Mann-Whitney test, and contingency table data were analyzed using a chi-square test. *P* values less than 0.05 were considered significant.

RESULTS

Confirmation of the critical TLR-7 genetic duplication. C57BL/6 β_2GPI$^{-/-}$ mice were derived by backcrossing 129/Sv × C57BL/6 β_2GPI$^{-/-}$ mice, which we previously generated (21), onto BXSB.*Yaa* and NZW WT mice (The Jackson Laboratory) for 10 generations. BXSB.*Yaa* refers to the male mice, and BXSB refers to female mice (which do not carry the YAA translocation). The NZW mice and the C57BL/6 mice served as controls. The absence of the β_2GPI gene in the

BXSB.*Yaa* β_2GPI$^{-/-}$ mice, the C57BL/6 β_2GPI$^{-/-}$ mice, and the NZW β_2GPI$^{-/-}$ mice was confirmed by PCR. The BXSB.*Yaa* mice, the NZW mice, the C57BL/6 WT mice, and the derived strains of β_2GPI$^{-/-}$ mice were all housed in the same environment under identical conditions and fed the same diet for the entirety of this study.

There is great variability in the literature regarding the time frame of disease onset in BXSB.*Yaa* WT mice (23–25). In view of the critical importance of TLR-7 gene duplication as the main genetic marker of the translocation (17), we assessed the TLR-7 gene copy number in the various groups of mice. The findings confirmed that the only difference between the BXSB.*Yaa* β_2GPI$^{-/-}$ mice and the BXSB.*Yaa* β_2GPI$^{+/+}$ mice in our cohort was the β_2GPI gene, and that the differences in phenotype between the 2 groups of mice could be attributed to this gene alone.

Effect of β_2GPI deletion on the degree of lymphoid hyperplasia, the severity of renal disease, and autoantibody production in TLR-7–dependent autoimmunity. *Submandibular and inguinal lymphadenopathy.* BXSB.*Yaa* β_2GPI$^{-/-}$ and BXSB.*Yaa* β_2GPI$^{+/+}$ mice were monitored for up to 36 weeks. Mice with clinically palpable submandibular lymphadenopathy and mice that were clinically unwell were killed. Among the BXSB.*Yaa* β_2GPI$^{-/-}$ mice, 72% developed massive submandibular lymphadenopathy and/or became unwell, whereas none of the BXSB.*Yaa* β_2GPI$^{+/+}$ mice developed these clinical features during the study ($P < 0.0001$ [n = 30/group]). The median age at which the BXSB.*Yaa* β_2GPI$^{-/-}$ mice became unwell was 19 weeks. Among the BXSB.*Yaa* β_2GPI$^{-/-}$ mice in which palpable lymphadenopathy developed, the mean ± SEM weight of the lymph node tissue (submandibular plus inguinal lymph nodes) was 269.4 ± 69.5 mg, and that of the BXSB.*Yaa* β_2GPI$^{+/+}$ mice was 10.4 ± 0.84 mg ($P < 0.03$ [n = 4]). Representative cervical lymph nodes from BXSB.*Yaa* β_2GPI$^{-/-}$ and BXSB.*Yaa* β_2GPI$^{+/+}$ mice are shown in Figure 1A. None of the female BXSB β_2GPI$^{-/-}$ and β_2GPI$^{+/+}$ mice and none of the male or female NZW, C57BL/6 β_2GPI$^{-/-}$, and β_2GPI$^{+/+}$ mice developed submandibular lymphadenopathy, and none died within the 36-week time frame.

Splenomegaly. A characteristic feature of lupus-prone BXSB.*Yaa* mice is splenomegaly (23). Both the size and weight of spleens from BXSB.*Yaa* β_2GPI$^{-/-}$ mice were significantly increased compared with the size and weight of spleens from BXSB.*Yaa* β_2GPI$^{+/+}$ mice (mean ± SEM 12.8 ± 2.7 versus 5.2 ± 0.7 mg/gm body weight; $P = 0.02$ [n = 7]). Representative spleens from BXSB.*Yaa* β_2GPI$^{-/-}$ and β_2GPI$^{+/+}$ mice are shown in Figure 1B. The male BXSB.*Yaa* control mice had splenomegaly, consistent with published reports of similarly aged (25 weeks) BXSB.*Yaa* mice (5.6 ± 0.5 mg/gm body weight) (23). As a point of comparison, the reported mean ± SEM weight of the spleens from similarly aged C57BL/6 mice was 2.4 ± 1.2 mg/gm body weight (23).

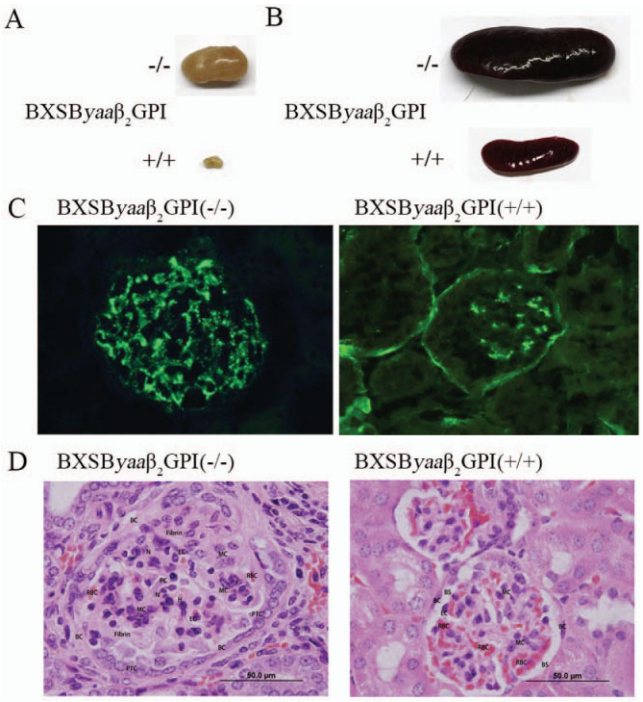

Figure 1. Lymphadenopathy, splenomegaly, and glomerulonephritis in BXSB.*Yaa* β_2-glycoprotein I–null (β_2GPI$^{-/-}$) mice. **A** and **B,** Representative cervical lymph nodes (**A**) and spleens (**B**) from BXSB.*Yaa* β_2GPI$^{-/-}$ mice and BXSB.*Yaa* β_2GPI$^{+/+}$ mice. **C** and **D,** Representative kidney sections from BXSB.*Yaa* β_2GPI$^{-/-}$ mice and BXSB.*Yaa* β_2GPI$^{+/+}$ mice, stained for C3 deposition (**C**) and with hematoxylin and eosin (**D**) (n = 5 mice in each group). In the hematoxylin and eosin–stained kidney sections from BXSB.*Yaa* β_2GPI$^{-/-}$ mice, the glomerulus shows mildly thickened Bowman's capsules (**BC**), hyperplastic mesangial cells (**MC**), capillary endothelial cells (**EC**), and red blood cells (**RBC**) within the capillaries. Inflammatory cells include neutrophils (**N**), possible histiocytes (**H**), and plasma cell (**PC**). The Bowman's space (**BS**) is obliterated by the expanded glomerular tuft, and proximal tubular epithelial cells (**PTC**) line some of the Bowman's capsular space. In the kidney sections from BXSB.*Yaa* β_2GPI$^{+/+}$ mice, the glomerulus shows normal Bowman's capsules, Bowman's space, mesangial cells, capillary endothelial cells, and red blood cells within the capillaries. Original magnification × 1,000. Color figure can be viewed in the online issue, which is available at http://onlinelibrary.wiley.com/doi/10.1002/art.38646/abstract.

Glomerulonephritis. BXSB.*Yaa* β_2GPI$^{-/-}$ mice had a more severe grade of glomerulonephritis compared with BXSB.*Yaa* β_2GPI$^{+/+}$ mice, as characterized by median scores for the severity of C3 deposition of 3

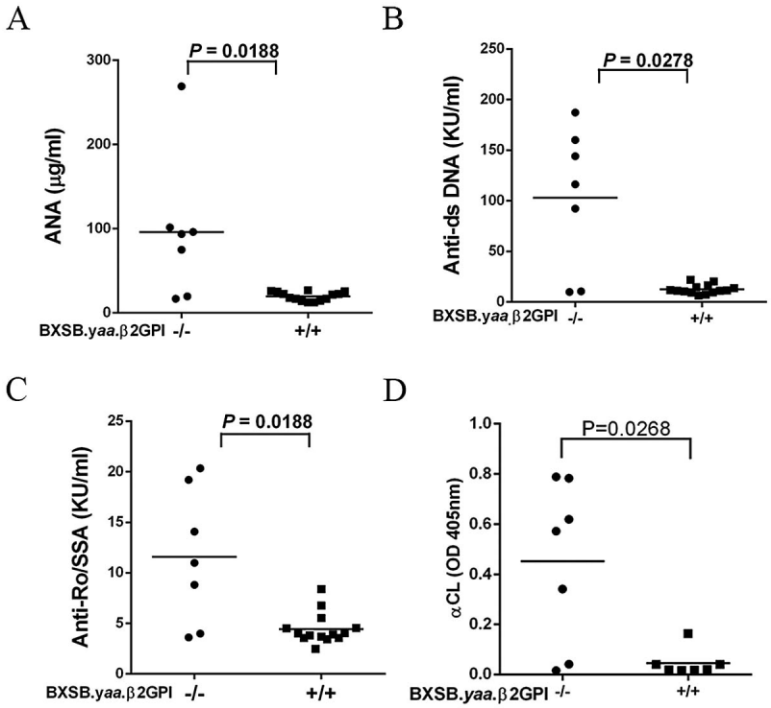

Figure 2. Levels of antinuclear antibodies (ANAs) (**A**), anti–double-stranded DNA (anti-dsDNA) (**B**), anti-Ro/SSA (**C**), and anticardiolipin autoantibodies (aCL) (**D**) in the serum of BXSB.*Yaa* β_2-glycoprotein I–null ($\beta_2GPI^{-/-}$) mice and BXSB.*Yaa* $\beta_2GPI^{+/+}$ mice, as determined using commercial enzyme-linked immunosorbent assays. Each data point represents a single mouse; horizontal lines show the mean. *P* values were calculated using the Mann-Whitney test. KU = Kunitz units.

and 1.5, respectively ($P = 0.008$ [n = 5]) and median scores for the severity of IgG deposition of 3 and 1, respectively ($P = 0.016$ [n = 5]). Representative kidney sections from BXSB.*Yaa* $\beta_2GPI^{-/-}$ and BXSB.*Yaa* $\beta_2GPI^{+/+}$ mice, stained for C3 deposition and with hematoxylin and eosin, respectively, are shown in Figures 1C and D. In the sections from BXSB.*Yaa* $\beta_2GPI^{-/-}$ mice, most glomeruli were hypercellular, and increased numbers of neutrophils, macrophages, and plasma cells as well as mesangial proliferation were observed, consistent with the histologic diagnosis of profuse proliferative glomerulonephritis. Fibrin plugs occluded the capillaries in some glomeruli. Many tubules were dilated and filled with protein-rich casts, and some were lined by flattened cells. In contrast, the glomeruli and tubules in specimens from the BXSB.*Yaa* $\beta_2GPI^{+/+}$ mice exhibited normal tissue architecture and cellular morphology.

Autoantibodies. Serum levels of autoantibodies were significantly higher in BXSB.*Yaa* $\beta_2GPI^{-/-}$ mice (n = 7) compared with BXSB.*Yaa* $\beta_2GPI^{+/+}$ mice (n = 14) (for ANAs, $P < 0.02$; for anti-dsDNA, $P < 0.03$; for anti-Ro/SSA, $P < 0.02$; for aCL, $P < 0.03$) (Figure 2). A marked increase in the level of autoantibodies to oxidized RNA was observed in BXSB.*Yaa* $\beta_2GPI^{-/-}$ mice compared with BXSB.*Yaa* $\beta_2GPI^{+/+}$ mice (mean ± SEM 2.90 ± 0.44 versus 0.22 ± 0.04 $OD_{405\ nm}$; $P = 0.0052$ [n = 5]). Anti-β_2GPI autoantibody levels were not elevated in either BXSB.*Yaa* $\beta_2GPI^{-/-}$ or BXSB.*Yaa* $\beta_2GPI^{+/+}$ mice (0.27 ± 0.13 versus 0.22 ± 0.17 $OD_{405\ nm}$; $P > 0.05$). The autoantibody levels in female BXSB $\beta_2GPI^{-/-}$ and BXSB $\beta_2GPI^{+/+}$ mice were not significantly different ($P = 0.1$ [n = 11]). Likewise, the ANA levels in the NZW $\beta_2GPI^{-/-}$, $\beta_2GPI^{+/+}$, C57BL/6 $\beta_2GPI^{-/-}$, and C57BL/6 $\beta_2GPI^{+/+}$ mice were not significantly different ($P > 0.05$ [n = 10]); the male and female mice within each strain were analyzed separately.

Marked potentiation of dysregulated leukocyte populations in TLR-7–dependent autoimmunity by β_2GPI deletion. All B cell and T cell subsets were expressed as a percentage relative to total lymphocytes, and the latter were defined based on the profiles of the forward and side scatter panels. Monocyte/macrophage/dendritic cell populations were expressed as a percentage relative to total cell numbers.

B cells. Cellular and histologic comparative analyses of spleen and lymph nodes from 5 independent age-matched pairs of BXSB.*Yaa* $\beta_2GPI^{-/-}$ and BXSB.*Yaa*

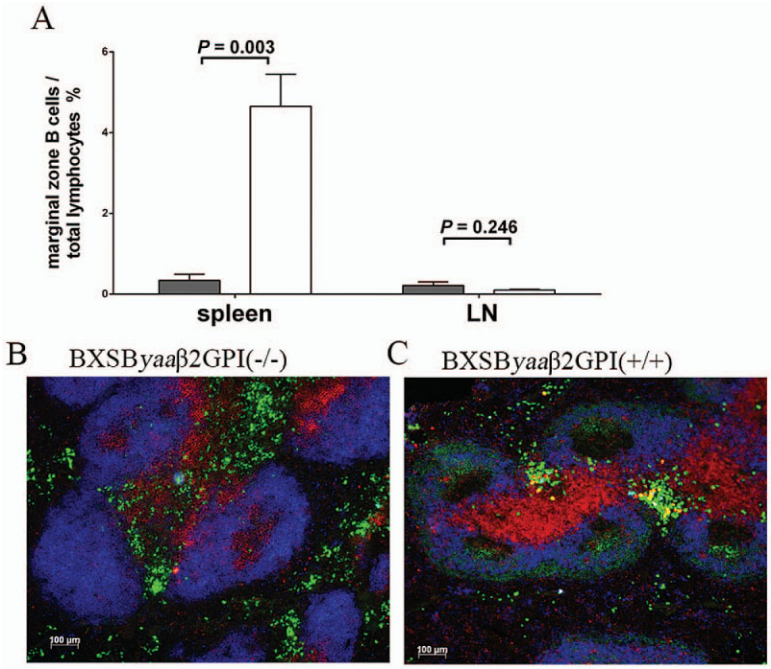

Figure 3. A, Percentages of marginal zone B cells in the spleen and lymph nodes (LNs) of age-matched BXSB.*Yaa* β_2-glycoprotein I–null (β_2GPI$^{-/-}$) mice (solid bars) and BXSB.*Yaa* β_2GPI$^{+/+}$ mice (open bars), as determined by fluorescence-activated cell sorting analysis. Values are the mean ± SEM of ≥4–5 independent pairs. *P* values were calculated using Student's *t*-test. **B** and **C,** Representative spleen sections from BXSB.*Yaa* β_2GPI$^{-/-}$ mice and BXSB.*Yaa* β_2GPI$^{+/+}$ mice, stained for B cell subsets and T cells using fluorescence-labeled antibodies. Blue staining (IgD) indicates follicular B cells, green staining (IgM) indicates marginal zone B cells, and red staining (CD3) indicates T cells.

β_2GPI$^{+/+}$ mice demonstrated that the former had an increased percentage of total B cells in the lymph nodes (mean ± SEM 51.67 ± 4.2% versus 28.38 ± 4.0%; P = 0.044 [n = 5]) and an increase in the follicular B cell population in the lymph nodes (42.5 ± 2.34 versus 26.88 ± 3.18%; P = 0.005 [n = 5]).

FACS analysis demonstrated that marginal zone B cells (CD23−CD21+B220+) were depleted in the spleens of BXSB.*Yaa* β_2GPI$^{-/-}$ mice compared with BXSB.*Yaa* controls (mean ± SEM 0.34 ± 0.1% versus 4.65 ± 0.8%; P = 0.003 [n = 5]) (Figure 3A). Representative spleen sections stained with fluorescence-

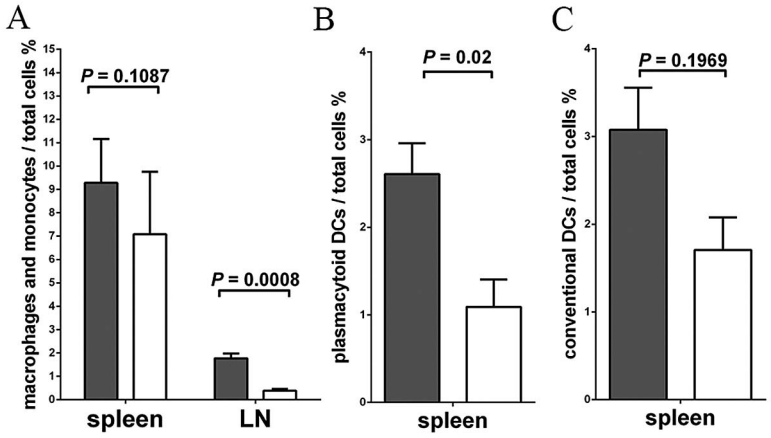

Figure 4. Percentages of monocyte/macrophages (CD11b+B220−) in the spleen and lymph nodes (**A**), plasmacytoid dendritic cells (DCs) (CD11c+ CD11b− B220+) in the spleen (**B**), and conventional dendritic cells (CD11c+CD11b+B220−) in the spleen (**C**) of age-matched β_2GPI$^{-/-}$ mice (solid bars) and BXSB.*Yaa* β_2GPI$^{+/+}$ mice (open bars), as determined by flow cytometry. Values are the mean ± SEM of ≥4–5 independent pairs. *P* values were calculated using Student's paired *t*-test. See Figure 3 for other definitions.

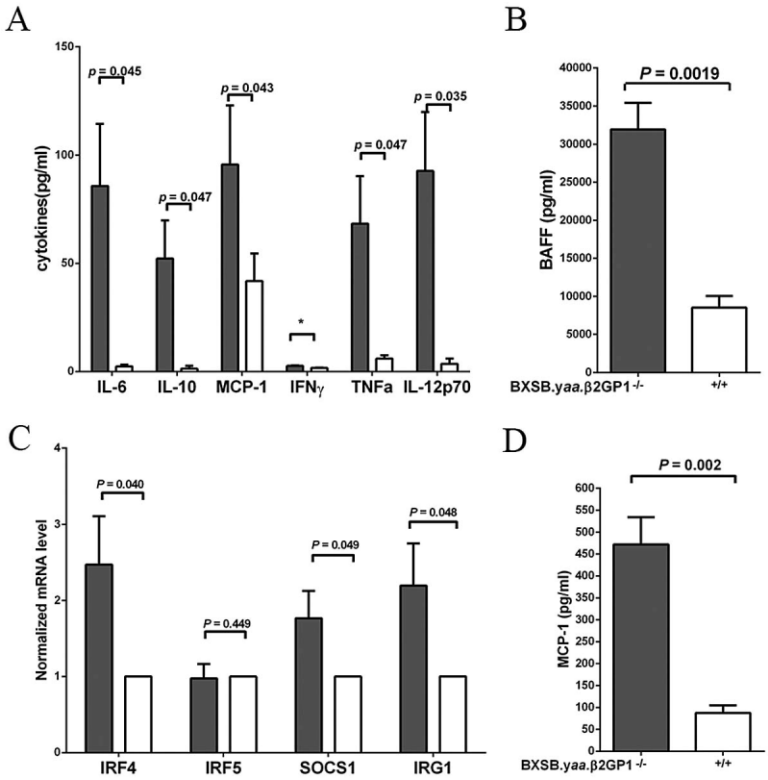

Figure 5. Effect of β_2-glycoprotein I (β_2GPI) deletion on the secretion of type I interferon (IFN), BAFF, and proinflammatory cytokines in β_2GPI$^{-/-}$ mice (solid bars) and age-matched BXSB.*Yaa* β_2GPI$^{+/+}$ mice (open bars). **A,** Levels of interleukin-6 (IL-6), IL-10, monocyte chemotactic protein 1 (MCP-1), IFNγ, tumor necrosis factor α (TNFα), and IL-12p70 in sera. $*$ = below the detection limit of the assay. **B,** Levels of BAFF in sera. **C,** Splenic expression of the signaling molecules associated with type I IFNs (IFN regulatory factor 4 [IRF-4], IRF-5, suppressor of cytokine signaling 1 [SOCS-1], and immunoresponsive gene 1 [IRG-1]). **D,** Secretion of MCP-1 after stimulation with the Toll-like receptor 7 agonist R848. Values are the mean ± SEM of 5 independent pairs. *P* values were calculated using Student's paired *t*-test.

labeled antibodies demonstrated the absence of marginal zone B cells in BXSB.*Yaa* β_2GPI$^{-/-}$ mice (Figures 3B and C).

Overexpression of TLR-7 was recently shown to be associated with a population of age-associated CD11c+ B cells in autoimmunity-prone mice (26,27). The percentage of cells consistent with age-associated B cells (CD23−CD21−B220+) was significantly increased in the spleens (mean ± SEM 13.87 ± 1.9% versus 7.53 ± 1.4%; $P = 0.013$ [n = 5]) and lymph nodes (8.58 ± 1.7% versus 1.89 ± 0.3%; $P = 0.011$ [n = 5]) of BXSB.*Yaa* β_2GPI$^{-/-}$ mice compared with paired age-matched BXSB.*Yaa* β_2GPI$^{+/+}$ mice. The proportion of transitional type 1 B cells (IgM+CD21−CD23−IgD+) was equal in the β_2GPI-knockout and control mice, in both the spleens and lymph nodes (data not shown). The percentage of activated B cells (CD69+B220+) was also significantly increased in the spleens (24.62 ± 3.25% versus 11.8 ± 1.56%; $P = 0.007$ [n = 5]) of BXSB.*Yaa* β_2GPI$^{-/-}$ mice compared with paired age-matched BXSB.*Yaa* WT mice.

Monocyte/macrophages and dendritic cells. The percentage of monocytes and macrophages was increased in the lymph nodes of BXSB.*Yaa* β_2GPI$^{-/-}$ mice (mean ± SEM 1.77 ± 0.2 versus 0.39 ± 0.06%; $P = 0.0008$ [n = 5]) (Figure 4A). The plasmacytoid dendritic cell population in the spleens of BXSB.*Yaa* β_2GPI$^{-/-}$ mice was expanded compared with that in the spleens of BXSB.*Yaa* β_2GPI$^{+/+}$ mice (2.60 ± 0.35% versus 1.09 ± 0.31%; $P = 0.02$ [n = 4]) (Figure 4B). There was no difference in the relative proportion of conventional splenic dendritic cells in the BXSB.*Yaa* β_2GPI$^{-/-}$ mice compared with the BXSB.*Yaa* β_2GPI$^{+/+}$ mice (Figure 4C).

T cells. The relative percentage of total T cells in the lymph nodes of BXSB.*Yaa* β_2GPI$^{-/-}$ mice was decreased compared with that in the lymph nodes of BXSB.*Yaa* β_2GPI WT mice (mean ± SEM 35.62 ± 4.78% versus 62.05 ± 5.13%; $P = 0.037$ [n = 5]). There

was no statistically significant difference in the relative populations of CD8+ T cells in either the spleens or lymph nodes of BXSB.*Yaa* β_2GPI$^{-/-}$ mice compared with BXSB.*Yaa* β_2GPI$^{+/+}$ mice. In contrast, there was enrichment of CD8+ effector memory T cells in the splenic tissue (0.95 ± 0.18% versus 0.22 ± 0.04%; P = 0.015 [n = 4]) and the lymph nodes (0.43 ± 0.18% versus 0.25 ± 0.15%; P = 0.020 [n = 4]) of BXSB.*Yaa* β_2GPI$^{-/-}$ mice. A higher proportion of CD8+ T cells expressed the activation marker CD69 in the spleens (37.58 ± 8.05% versus 9.71 ± 2.39%; P = 0.028 [n = 5]) and lymph nodes (24.16 ± 4.19% versus 10.27 ± 1.78%; P = 0.042 [n = 5]) of BXSB.*Yaa* β_2GPI$^{-/-}$ mice compared with BXSB.*Yaa* β_2GPI$^{+/+}$ mice.

The percentage of total CD4+ T cells was decreased in the spleens (mean ± SEM 12.68 ± 1.6% versus 14.68 ± 1.8%; P = 0.023 [n = 4]) and lymph nodes (22.90 ± 3.24% versus 33.73 ± 1.74%; P = 0.045 [n = 4]) of BXSB.*Yaa* β_2GPI$^{-/-}$ mice compared with BXSB.*Yaa* β_2GPI$^{+/+}$ mice.

The percentages of effector memory T cells in the spleens of BXSB.*Yaa* β_2GPI$^{-/-}$ mice and BXSB.*Yaa* β_2GPI$^{+/+}$ mice were 7.93 ± 0.92% and 3.40 ± 0.25%, respectively (P = 0.018 [n = 4]), and the percentages in lymph nodes were 8.29 ± 1.13% and 2.35 ± 0.29%, respectively (P = 0.014 [n = 4]). A similar trend was seen with activated CD4+ T cells in the spleens (26.47 ± 6.43% versus 13.12 ± 2.96%; P = 0.026 [n = 5]) and lymph nodes (19.9 ± 4.06% versus 12.19 ± 2.82%; P = 0.036 [n = 5]).

Effect of β_2GPI deletion on secretion of type I IFN, BAFF, and proinflammatory cytokines in TLR-7–dependent autoimmunity. Significantly elevated levels of IL-6, IL-10, MCP-1, TNFα, and IL-12p70 were detected in the sera of BXSB.*Yaa* β_2GPI$^{-/-}$ mice compared with age-matched BXSB.*Yaa* β_2GPI$^{+/+}$ mice ($P < 0.05$ for all cytokines [n = 5]) (Figure 5A). The level of BAFF, a cytokine that promotes increased B cell activation and survival (28), was greatly increased in the sera of BXSB.*Yaa* β_2GPI$^{-/-}$ mice compared with BXSB.*Yaa* β_2GPI$^{+/+}$ mice (31,936 ± 3,479 pg/ml versus 8,532 ± 1,529 pg/ml; P = 0.0019 [n = 5]) (Figure 5B). The mean BAFF level in the sera of BXSB.*Yaa* β_2GPI$^{+/+}$ mice agreed precisely with previously reported levels (29). Expression analysis of complementary DNA from the splenocytes of BXSB.*Yaa* β_2GPI$^{-/-}$ mice compared with those from BXSB.*Yaa* β_2GPI$^{+/+}$ mice showed a significant increase in the expression of IRF-4, SOCS-1, and IRG-1 ($P < 0.05$ [n = 5]) (Figure 5C), consistent with an increase in the type I IFN signature using the method described by Deane et al (22). Stimulation of splenocytes with the TLR-7 agonist R848/resiquimod resulted in profound stimulation and secretion of MCP-1 in BXSB.*Yaa* β_2GPI$^{-/-}$ mice compared with BXSB.*Yaa* β_2GPI$^{+/+}$ mice (mean ± SEM 472.1 ± 61.94 pg/ml versus 87.58 ± 16.92 pg/ml; P = 0.002 [n = 5]) (Figure 5D).

Impairment of apoptotic cell clearance by β_2GPI deletion. We assessed in vivo phagocytosis of apoptotic cells by peritoneal macrophages in BXSB.*Yaa* β_2GPI$^{-/-}$ mice compared with BXSB.*Yaa* β_2GPI$^{+/+}$ mice. In β_2GPI$^{-/-}$ mice, the percentage of apoptotic cells phagocytosed within a set time frame was significantly lower than that in controls (mean ± SEM 55.04 ± 3.48% versus 81.74 ± 3.43%; P = 0.0006 [n = 5]).

DISCUSSION

In this study, we discuss the novel concept that deletion of β_2GPI leads to potentiation of the lupus phenotype in male BXSB.*Yaa* mice. These findings suggest that β_2GPI most likely interacts with one or perhaps multiple other gene products coded on the translocation that serves to attenuate the lupus phenotype. There are at least 17 genes on the YAA translocation. Therefore, delineating precisely how β_2GPI influences the phenotype will be a major undertaking and is beyond the scope of the current study, which was intended to describe a novel phenotype. However, we did explore a number of possible mechanisms by which β_2GPI may be able to regulate the BXSB.*Yaa* lupus phenotype based on our understanding of the physiologic functions of β_2GPI.

β_2GPI in the free thiol form serves an antioxidant function, protecting cells against oxidative stress–induced apoptosis (7). Hence, we hypothesize that in BXSB.*Yaa* β_2GPI$^{-/-}$ mice, there is less buffering of free radicals, leading to a heightened free radical load. This may then contribute to the creation of oxidation-mediated neoepitopes on apotopes (endogenous autoantigens expressed on the surface of apoptotic cells, with Ro 60 being one example [8]), leading to a heightened and accelerated autoimmune response. Oxidative stress has previously been shown to induce posttranslational modifications of endogenous autoantigens to create neoepitopes that are more immunogenic and elicit an augmented autoimmune response (30). This has been studied in detail with regard to Ro 60, which is composed of 60-kd RNPs noncovalently associated with at least 1 of 4 short uridine-rich RNAs (the hyRNAs) (31). Oxidative modification of Ro 60 resulted in the acceleration of epitope spreading compared with nonoxidized

Ro 60, when both oxidized and nonoxidized Ro 60 were used to immunize rabbits (31).

These findings may have relevance in explaining the amplified autoimmune response seen in BXSB.*Yaa* β_2GPI$^{-/-}$ mice compared with that in BXSB.*Yaa* β_2GPI$^{+/+}$ mice. This notion is supported by the higher levels of autoantibodies to oxidized RNA in BXSB.*Yaa* β_2GPI$^{-/-}$ mice compared with WT mice. It is plausible, although not proven, that high titers of immune complexes containing RNA moieties may drive the amplified autoimmune response in BXSB.*Yaa* β_2GPI$^{-/-}$ mice, in view of the documented in vitro ability of RNA-containing immune complexes to activate B cells and plasmacytoid DCs via dual engagement of Fcγ receptor and TLR-7 (20,32).

The levels of anticardiolipin autoantibodies (those binding negatively charged phospholipids), in addition to ANAs, anti-dsDNA, and anti-Ro autoantibodies, were elevated in BXSB.*Yaa* β_2GPI$^{-/-}$ mice compared with WT mice, which is consistent with potentiation of the autoimmune response. This autoantibody profile is detected several years prior to the onset of clinical SLE in humans (33).

Previous studies have demonstrated that β_2GPI binds to apoptotic cell surfaces in vitro and in vivo (9), and in vitro studies suggest that opsonization of apoptotic cells by β_2GPI may mediate a role in enhancing apoptotic cell clearance by macrophages (10). Increased apoptosis and impaired apoptotic cell clearance are relevant mechanisms contributing to the pathogenesis of lupus (34,35). In this study, we demonstrated, using an in vivo model, that apoptotic cell clearance was impaired in BXSB.*Yaa* β_2GPI$^{-/-}$ mice compared with WT mice. Hence, an increase in the generation of apoptotic cells and the impairment of apoptotic cell clearance as a result of β_2GPI deletion may also be important factors accounting for the accentuated lupus phenotype in BXSB.*Yaa* β_2GPI$^{-/-}$ mice.

β_2GPI has previously been shown to localize in the late endosome of cells (36), the same intracellular location as that of TLR-7. This raises the possibility that β_2GPI may be able to directly inhibit the ability of small RNP-containing immune complexes (e.g., Sm and Ro/SSA) from activating TLR-7 receptors within plasmacytoid DCs and autoimmune B cells, thus abrogating type I IFN secretion, which previous studies have shown to be an important positive feedback loop in sustaining the production of such autoantibodies and the murine lupus phenotype (37). In this study, we showed that the type I IFN signature is diminished in BXSB.*Yaa* β_2GPI$^{+/+}$ mice compared with BXSB.*Yaa* β_2GPI$^{-/-}$ mice, and in conjunction with this, that the titers of anti-Ro/SSA and antioxidized RNA are lower in the former group compared with the latter.

We previously demonstrated that β_2GPI binds to Ro 60 on the surface of late apoptotic cells and inhibits the ability of pathogenic anti–Ro 60 autoantibodies to form immune complexes (8). This observation raises the possibility that another mechanism through which β_2GPI may attenuate BXSB.*Yaa* autoimmunity is via inhibiting the formation of anti–Ro 60 immune complexes in these mice. In vitro studies using human autoantibodies have shown that once such anti–Ro 60 immune complexes form, they are able to activate TLR-7, which may ultimately be the mechanism responsible for the scarring inflammation that leads to congenital heart block in neonatal lupus (38).

A mechanistic link was recently established between antiphospholipid antibodies and abnormal TLR-7 and TLR-8 activation (39). IgG fractions from patients with APS were shown to localize to the late endosome of plasmacytoid DCs and monocytes, up-regulate the expression of TLR-7/8, and potentiate their activity, leading to heightened secretion of type I IFN and several other proinflammatory cytokines in vitro (39). These antibody-mediated effects depended on the activation of NADPH oxidase and the generation of superoxide (39). We speculate that intracellular localizing antibodies from patients with APS may disrupt the TLR-7/8–type I IFN axis in plasmacytoid DCs and monocytes (39), perhaps by antagonizing a physiologic intracellular TLR-7 inhibitory function of β_2GPI.

In summary, we have described our finding of the development of an accelerated and potentiated autoimmune lupus phenotype in male BXSB.*Yaa* mice in which β_2GPI has been deleted. This finding may have implications for furthering our understanding of the pathogenic mechanisms of several distinct autoimmune syndromes in which TLR-7 has been implicated, including SLE, APS, and congenital heart block associated with anti–Ro 60 autoantibodies.

AUTHOR CONTRIBUTIONS

All authors were involved in drafting the article or revising it critically for important intellectual content, and all authors approved the final version to be published. Dr. Krilis had full access to all of the data in the study and takes responsibility for the integrity of the data and the accuracy of the data analysis.

Study conception and design. Giannakopoulos, Mirarabshahi, Krilis.

Acquisition of data. Giannakopoulos, Mirarabshahi, M. Qi, Weatherall, J. C. Qi, Tanaka, Millar, Vonthethoff, Gatto, Spielman, Krilis.

Analysis and interpretation of data. Giannakopoulos, Mirarabshahi, M. Qi, Weatherall, J. C. Qi, Tanaka, Millar, Vonthethoff, Gatto, Spielman, Krilis.

REFERENCES

1. Miyakis S, Lockshin MD, Atsumi T, Branch DW, Brey RL, Cervera R, et al. International consensus statement on an update of the classification criteria for definite antiphospholipid syndrome (APS). J Thromb Haemost 2006;4:295–306.
2. Giannakopoulos B, Krilis SA. The pathogenesis of the antiphospholipid syndrome. N Engl J Med 2013;368:1033–44.
3. McNeil HP, Simpson RJ, Chesterman CN, Krilis SA. Antiphospholipid antibodies are directed against a complex antigen that includes a lipid-binding inhibitor of coagulation: β2-glycoprotein I (apolipoprotein H). Proc Natl Acad Sci U S A 1990;87:4120–4.
4. Miyakis S, Giannakopoulos B, Krilis SA. Beta 2 glycoprotein I: function in health and disease. Thromb Res 2004;114:335–46.
5. Passam FH, Rahgozar S, Qi M, Raftery MJ, Wong JW, Tanaka K, et al. Beta 2 glycoprotein I is a substrate of thiol oxidoreductases. Blood 2010;116:1995–7.
6. Ioannou Y, Zhang JY, Qi M, Gao L, Qi JC, Yu DM, et al. Novel assays of thrombogenic pathogenicity in the antiphospholipid syndrome based on the detection of molecular oxidative modification of the major autoantigen β_2-glycoprotein I. Arthritis Rheum 2011;63:2774–82.
7. Ioannou Y, Zhang JY, Passam FH, Rahgozar S, Qi JC, Giannakopoulos B, et al. Naturally occurring free thiols within β2-glycoprotein I in vivo: nitrosylation, redox modification by endothelial cells, and regulation of oxidative stress-induced cell injury. Blood 2010;116:1961–70.
8. Reed JH, Giannakopoulos B, Jackson MW, Krilis SA, Gordon TP. Ro 60 functions as a receptor for β_2-glycoprotein I on apoptotic cells. Arthritis Rheum 2009;60:860–9.
9. Balasubramanian K, Maiti SN, Schroit AJ. Recruitment of β-2-glycoprotein 1 to cell surfaces in extrinsic and intrinsic apoptosis. Apoptosis 2005;10:439–46.
10. Maiti SN, Balasubramanian K, Ramoth JA, Schroit AJ. Beta-2-glycoprotein 1-dependent macrophage uptake of apoptotic cells: binding to lipoprotein receptor-related protein receptor family members. J Biol Chem 2008;283:3761–6.
11. Cervera R, Piette JC, Font J, Khamashta MA, Shoenfeld Y, Camps MT, et al. Antiphospholipid syndrome: clinical and immunologic manifestations and patterns of disease expression in a cohort of 1,000 patients. Arthritis Rheum 2002;46:1019–27.
12. Bruce IN, Clark-Soloninka CA, Spitzer KA, Gladman DD, Urowitz MB, Laskin CA. Prevalence of antibodies to β2-glycoprotein I in systemic lupus erythematosus and their association with antiphospholipid antibody syndrome criteria: a single center study and literature review. J Rheumatol 2000;27:2833–7.
13. Hashimoto Y, Kawamura M, Ichikawa K, Suzuki T, Sumida T, Yoshida S, et al. Anticardiolipin antibodies in NZW x BXSB F1 mice: a model of antiphospholipid syndrome. J Immunol 1992;149:1063–8.
14. Monestier M, Kandiah DA, Kouts S, Novick KE, Ong GL, Radic MZ, et al. Monoclonal antibodies from NZW x BXSB F1 mice to β2 glycoprotein I and cardiolipin: species specificity and charge-dependent binding. J Immunol 1996;156:2631–41.
15. Reddel SW, Wang YX, Sheng YH, Krilis SA. Epitope studies with anti-β2-glycoprotein I antibodies from autoantibody and immunized sources. J Autoimmun 2000;15:91–6.
16. Ida A, Hirose S, Hamano Y, Kodera S, Jiang Y, Abe M, et al. Multigenic control of lupus-associated antiphospholipid syndrome in a model of (NZW x BXSB) F1 mice. Eur J Immunol 1998;28:2694–703.
17. Pisitkun P, Deane JA, Difilippantonio MJ, Tarasenko T, Satterthwaite AB, Bolland S. Autoreactive B cell responses to RNA-related antigens due to TLR7 gene duplication. Science 2006;312:1669–72.
18. Subramanian S, Tus K, Li QZ, Wang A, Tian XH, Zhou J, et al. A Tlr7 translocation accelerates systemic autoimmunity in murine lupus. Proce Nat Acad Sci U S A. 2006;103:9970–5.
19. Lau CM, Broughton C, Tabor AS, Akira S, Flavell RA, Mamula MJ, et al. RNA-associated autoantigens activate B cells by combined B cell antigen receptor/Toll-like receptor 7 engagement. J Exp Med 2005;202:1171–7.
20. Vollmer J, Tluk S, Schmitz C, Hamm S, Jurk M, Forsbach A, et al. Immune stimulation mediated by autoantigen binding sites within small nuclear RNAs involves Toll-like receptors 7 and 8. J Exp Med 2005;202:1575–85.
21. Sheng Y, Reddel SW, Herzog H, Wang YX, Brighton T, France MP, et al. Impaired thrombin generation in β2-glycoprotein I null mice. J Biol Chem 2001;276:13817–21.
22. Deane JA, Pisitkun P, Barrett RS, Feigenbaum L, Town T, Ward JM, et al. Control of toll-like receptor 7 expression is essential to restrict autoimmunity and dendritic cell proliferation. Immunity 2007;27:801–10.
23. Murphy ED, Roths JB. A Y chromosome associated factor in strain BXSB producing accelerated autoimmunity and lymphoproliferation. Arthritis Rheum 1979;22:1188–94.
24. McPhee CG, Sproule TJ, Shin DM, Bubier JA, Schott WH, Steinbuck MP, et al. MHC class I family proteins retard systemic lupus erythematosus autoimmunity and B cell lymphomagenesis. J Immunol 2011;187:4695–704.
25. Kubo C, Gajar A, Johnson BC, Good RA. The effects of dietary restriction on immune function and development of autoimmune disease in BXSB mice. Proc Natl Acad Sci U S A 1992;89:3145–9.
26. Rubtsov AV, Rubtsova K, Fischer A, Meehan RT, Gillis JZ, Kappler JW, et al. Toll-like receptor 7 (TLR7)-driven accumulation of a novel CD11c(+) B-cell population is important for the development of autoimmunity. Blood 2011;118:1305–15.
27. Hao Y, O'Neill P, Naradikian MS, Scholz JL, Cancro MP. A B-cell subset uniquely responsive to innate stimuli accumulates in aged mice. Blood 2011;118:1294–304.
28. Mackay F, Schneider P. Cracking the BAFF code. Nat Rev Immunol 2009;9:491–502.
29. Ding H, Wang L, Wu X, Yan J, He Y, Ni B, et al. Blockade of B-cell-activating factor suppresses lupus-like syndrome in autoimmune BXSB mice. J Cell Mol Med 2010;14:1717–25.
30. Kurien BT, Scofield RH. Autoimmunity and oxidatively modified autoantigens. Autoimmun Rev 2008;7:567–73.
31. Scofield RH, Kurien BT, Ganick S, McClain MT, Pye Q, James JA, et al. Modification of lupus-associated 60-kDa Ro protein with the lipid oxidation product 4-hydroxy-2-nonenal increases antigenicity and facilitates epitope spreading. Free Radic Biol Med 2005;38:719–28.
32. Savarese E, Chae OW, Trowitzsch S, Weber G, Kastner B, Akira S, et al. U1 small nuclear ribonucleoprotein immune complexes induce type I interferon in plasmacytoid dendritic cells through TLR7. Blood 2006;107:3229–34.
33. Arbuckle MR, McClain MT, Rubertone MV, Scofield RH, Dennis GJ, James JA, et al. Development of autoantibodies before the clinical onset of systemic lupus erythematosus. N Engl J Med 2003;349:1526–33.
34. Emlen W, Niebur J, Kadera R. Accelerated in vitro apoptosis of lymphocytes from patients with systemic lupus erythematosus. J Immunol 1994;152:3685–92.
35. Cohen PL, Caricchio R, Abraham V, Camenisch TD, Jennette JC, Roubey RA, et al. Delayed apoptotic cell clearance and lupus-like autoimmunity in mice lacking the c-mer membrane tyrosine kinase. J Exp Med 2002;196:135–40.
36. Dunoyer-Geindre S, Kruithof EK, Galve-de Rochemonteix B, Rosnoblet C, Gruenberg J, Reber G, et al. Localization of β2-glycoprotein 1 in late endosomes of human endothelial cells. Thromb Haemost 2001;85:903–7.
37. Christensen SR, Shupe J, Nickerson K, Kashgarian M, Flavell RA,

Shlomchik MJ. Toll-like receptor 7 and TLR9 dictate autoantibody specificity and have opposing inflammatory and regulatory roles in a murine model of lupus. Immunity 2006;25:417–28.
38. Clancy RM, Alvarez D, Komissarova E, Barrat FJ, Swartz J, Buyon JP. Ro60-associated single-stranded RNA links inflammation with fetal cardiac fibrosis via ligation of TLRs: a novel pathway to autoimmune-associated heart block. J Immunol 2010; 184:2148–55.
39. Prinz N, Clemens N, Strand D, Putz I, Lorenz M, Daiber A, et al. Antiphospholipid antibodies induce translocation of TLR7 and TLR8 to the endosome in human monocytes and plasmacytoid dendritic cells. Blood 2011;118:2322–32.

DOI 10.1002/art.38649

Clinical Images: Actinomycetoma of the foot

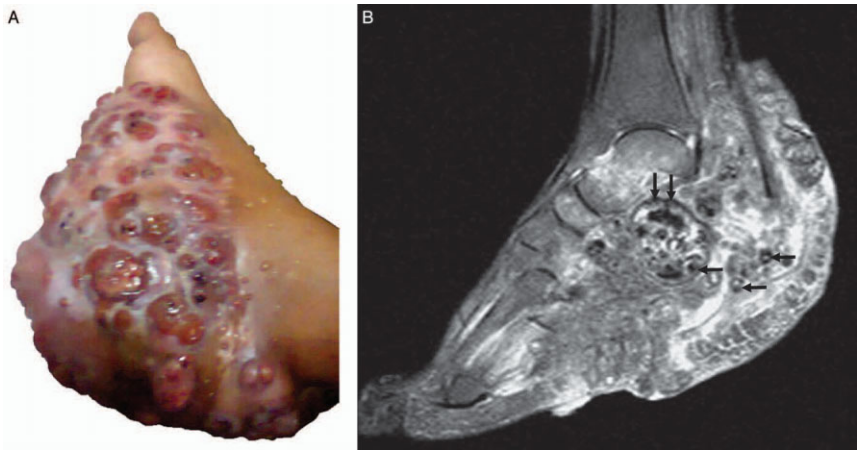

The patient, a 33-year-old woman, presented with swelling and pain in the right foot, which had increased progressively over the last 3 years, with a history of contusional trauma before the onset of symptoms. Clinical examination showed swelling involving mainly the right midfoot and hindfoot, associated with discharging sinuses and black grains (**A**). T2-weighted, fat-suppressed sagittal magnetic resonance imaging (MRI) revealed a large heterogeneous mass involving the soft tissue and bones of the plantar midfoot and hindfoot (**B**). Multiple small, spherical, hyperintense lesions with peripheral hypointense rims were distributed diffusely in the synovial tissue. These lesions exhibited tiny central hypointense foci suggestive of the "dot-in-circle" sign (**arrows**). The patient underwent amputation of the foot, and a diagnosis of mycetoma was confirmed by the presence of *Actinomyces* seen on histopathologic analysis. Mycetoma was first described in the Madurai district of southern India (1); hence, the eponym "Madura foot." This chronic granulomatous disease is caused by *Actinomyces* bacteria (actinomycetoma) or true fungi (eumycetoma). MRI shows the "dot-in-circle" sign (2), which refers to the presence of small, round, hyperintense lesions surrounded by low-signal-intensity rims with central foci of low signal intensity. This finding represents the clustering of the organism, known as "grains," which are found within abscesses surrounded by granulation tissue. The sign is specific for mycetoma, and MRI can provide an early diagnosis of the disease (3). Furthermore, these fastidious organisms may be difficult to demonstrate by biopsy or microbiologic culture. Antimicrobial therapy is sometimes curative for mycetoma involving the soft tissue. However, amputation may be required in cases of bony involvement, as in the patient described herein.

1. Kumar J, Kumar A, Sethy P, Gupta S. The dot-in-circle sign of mycetoma on MRI. Diagn Interv Radiol 2007;13:193–5.
2. Cherian RS, Betty M, Manipadam MT, Cherian VM, Poonnoose PM, Oommen AT, et al. The "dot-in-circle" sign—a characteristic MRI finding in mycetoma foot: a report of three cases. Br J Radiol 2009;82:662–5.
3. Sharif HS, Clark DC, Aabed MY, Aideyan OA, Mattsson TA, Haddad MC, et al. Mycetoma: comparison of MR imaging with CT. Radiology 1991;178:865–70.

Augusto Altoé, MD
Silvana Mendonça, MD
Guilherme Taboada, MD
Clínica de Diagnóstico por Imagem
Clarissa Canella, MD
Flávia Costa, MD
Clínica de Diagnóstico por Imagem and Universidade Federal do Rio de Janeiro
Edson Marchiori, PhD
Universidade Federal do Rio de Janeiro
Rio de Janeiro, Brazil